ARMY RESEARCH LABORATORY

A High Resolution, Three-Dimensional, Computationally Efficient, Diagnostic Wind Model: Initial Development Report

by Yansen Wang, Jon J. Mercurio, Chatt C. Williamson, Dennis M. Garvey and Sam Chang

ARL-TR-3094 **October 2003**

Report Documentation Page

Form Approved
OMB No. 0704-0188

1. REPORT DATE	2. REPORT TYPE	3. DATES COVERED
00 SEP 2003	**N/A**	**-**

4. TITLE AND SUBTITLE	5a. CONTRACT NUMBER
A High Resolution, Three-Dimensional, Computationally Efficient, Diagnostic Wind Model: Initial Development Report	5b. GRANT NUMBER
	5c. PROGRAM ELEMENT NUMBER
6. AUTHOR(S)	5d. PROJECT NUMBER
	5e. TASK NUMBER
	5f. WORK UNIT NUMBER
7. PERFORMING ORGANIZATION NAME(S) AND ADDRESS(ES) **U.S. Army Research Lab., ATTN: AMSRL-CI-EB, 2800 Powder Mill Rd., Adelphi, MD 20783-1197**	8. PERFORMING ORGANIZATION REPORT NUMBER
9. SPONSORING/MONITORING AGENCY NAME(S) AND ADDRESS(ES)	10. SPONSOR/MONITOR'S ACRONYM(S)
	11. SPONSOR/MONITOR'S REPORT NUMBER(S)

12. DISTRIBUTION/AVAILABILITY STATEMENT
Approved for public release, distribution unlimited

13. SUPPLEMENTARY NOTES
The original document contains color images.

14. ABSTRACT

15. SUBJECT TERMS

16. SECURITY CLASSIFICATION OF:			17. LIMITATION OF ABSTRACT	18. NUMBER OF PAGES	19a. NAME OF RESPONSIBLE PERSON
a. REPORT	b. ABSTRACT	c. THIS PAGE			
unclassified	**unclassified**	**unclassified**	**UU**	**28**	

Standard Form 298 (Rev. 8-98)
Prescribed by ANSI Std Z39-18

NOTICES

Disclaimers

The findings in this report are not to be construed as an official Department of the Army position unless so designated by other authorized documents.

Citation of manufacturer's or trade names does not constitute an official endorsement or approval of the use thereof.

Destroy this report when it is no longer needed. Do not return it to the originator.

Army Research Laboratory
Adelphi, MD 20783-1197

ARL-TR-3094 **October 2003**

A High Resolution, Three-Dimensional, Computationally Efficient, Diagnostic Wind Model: Initial Development Report

Yansen Wang, Jon J. Mercurio, Chatt C. Williamson, Dennis M. Garvey, and Sam Chang
Computational and Information Sciences Directorate, ARL

REPORT DOCUMENTATION PAGE

Form Approved
OMB No. 0704-0188

1. REPORT DATE *(DD-MM-YYYY)*	2. REPORT TYPE	3. DATES COVERED (From - To)
October 2003	Final	FY2003

4. TITLE AND SUBTITLE
A High Resolution, Three-Dimensional, Computationally Efficient, Diagnostic Wind Model: Initial Development Report

5a. CONTRACT NUMBER

5b. GRANT NUMBER

5c. PROGRAM ELEMENT NUMBER

6. AUTHOR(S)
Yansen Wang, Jon J. Mercurio, Chatt C. Williamson, Dennis M. Garvey, and Sam Chang

5d. PROJECT NUMBER
3FEJ00

5e. TASK NUMBER

5f. WORK UNIT NUMBER

7. PERFORMING ORGANIZATION NAME(S) AND ADDRESS(ES)
U.S. Army Research Laboratory
ATTN: AMSRL-CI-EB
2800 Powder Mill Road
Adelphi, MD 20783-1197

8. PERFORMING ORGANIZATION REPORT NUMBER
ARL-TR-3094

9. SPONSORING/MONITORING AGENCY NAME(S) AND ADDRESS(ES)
U.S. Army Research Laboatory
2800 Powder Mill Road
Adelphi, MD 20783-1197

10. SPONSOR/MONITOR'S ACRONYM(S)

11. SPONSOR/MONITOR'S REPORT NUMBER(S)

12. DISTRIBUTION/AVAILABILITY STATEMENT
Approved for public release; distribution unlimited.

13. SUPPLEMENTARY NOTES

14. ABSTRACT
This document describes a three-dimensional, high resolution, computationally efficient, diagnostic model for flow over complex terrain using a mass consistent approach. The differences between the current model and similar approaches are (a) the lower boundary conditions and (b) an efficient numerical method. The model includes the effects of topography and small surface features such as forest areas and buildings on the overall flow. The numerical implementation takes advantage of a multigrid method that greatly improves the computation speed. The framework of the model and associated implementations are described here. Several preliminary test cases for the model are also given in this documentation.

15. SUBJECT TERMS
Diagnostic wind model, wind in complex terrain, urban wind model

16. SECURITY CLASSIFICATION OF:			17. LIMITATION OF ABSTRACT	18. NUMBER OF PAGES	19a. NAME OF RESPONSIBLE PERSON
a. REPORT	b. ABSTRACT	c. THIS PAGE	UL	26	Yansen Wang
Unclassified	Unclassified	Unclassified			19b. TELEPHONE NUMBER (*Include area code*) 301-394-1310

Standard Form 298 (Rev. 8/98)
Prescribed by ANSI Std. Z39.18

Contents

List of Figures iv

List of Tables iv

1. Introduction 1

2. Model Description 3

2.1 Variational Formulation 3

2.2 Vertical Coordinate 4

2.3 Treatment of the Turbulent Surface Layer 5

2.4 Partitioning the Flow Using the Richardson Number 6

3. Numerical Methods 6

3.1 Finite Difference Discretization 6

3.2 Multigrid Method 7

4. Initial Test Results of the Model 10

4.1 Test With the Potential Flow Solutions....10

4.2 Flow Around and Over Building Blocks....13

4.3 Computational Efficiency of the Model....16

5. Summary and Conclusions 17

References 18

Distribution List 21

List of Figures

Figure 1. A schematic illustration of variable step vertical coordinate 5

Figure 2. Comparison of the potential flow analytical solution (left panel figures) with the numerical model solution (right panel figures). (The top panels are the horizontal cross sections at z = 1.55 km. The bottom panels are the vertical cross sections at y = 5 km) 12

Figure 3. Streamlines of flow around infinite long half cylinder ridge (top panel); streamlines of flow over a 2-D Witch-of-Agnesi ridge (bottom panel).....13

Figure 4. A schematic graph shows the mean flow pattern over and around a wall-mounted box.....14

Figure 5. 3DSTAT simulation of wind flow around and over 3-D building blocks. (The top panel is a horizontal cross section at z = 5m, and the bottom panel is a vertical cross section at y = 30m).....15

Figure 6. Flow over a 3-D block array. (3DSTAT simulation (top panel) and the wind tunnel data (bottom panel, U.S. EPA)) 16

List of Tables

Table 1. Comparison of CPU time (minutes) with different numerical methods.....17

1. Introduction

Numerical modeling of transport and diffusion, or the analysis of atmospheric effects on the performance of sensors, requires wind data with high spatial (10 to 100 meters) and temporal (2 to 5 minutes) resolution across a reasonably large (10 x 10 km) domain. Traditionally, there have been two approaches to generate such high resolution wind fields, and both rely on computer numerical modeling of the atmosphere. The engineering and atmospheric sciences communities usually simulate the wind field in an urban area by extending their computational fluid dynamic (CFD) or large eddy simulation (LES) models for laboratory control environmental conditions. Those models have advantages in that their detailed treatment of complex surface morphologies allow for improved simulations of the flow field structure. However, LES models are generally not designed to accurately account for the deep atmospheric structures that are the major driving force for the small scale flows. The computational expense for this type of model is too large to cover a reasonably sized urban area. On the other hand, atmospheric numerical weather prediction (NWP) models usually attempt to represent a variety of natural flow scales and phenomena including turbulence, gravity waves, deep convection, fronts, and long waves. Either by increasing the NWP model resolution directly or alternately by nesting a large eddy simulation model within a mesoscale NWP model, one can provide mean values and associated turbulence statistics, which are potential solutions for the requirement. Unfortunately, it remains impractical for real-time applications in the foreseeable future because of the limitations of available computer power. Besides the huge requirement of computational resources, the predictability of the forecast model in microscale remains debatable and is in need of further research. For applications requiring a combination of rapid and accurate results, a well-designed diagnostic model, which is exercised at specific times over limited domains, may provide a solution.

One particular type of diagnostic model that satisfies some physical or dynamical constraints is explored in this study. The theoretical basis for this type of model was developed by Sasaki (1958; 1970) using variational analysis. The general variational analysis defines an integral function whose solution minimizes the variance of the difference between the observed and analyzed variable values, subject to physical constraints. The physical constraints may be any combination of the mass, momentum, and energy conservation equations. If the physical constraints are all three conservation equations, the problem becomes effectively a three-dimensional variational data assimilation problem. Obviously, this approach becomes increasingly more computationally intensive as constraints are added because one not only has to solve the constraint equations but also has to minimize the difference between the observations and the results from the prediction model. If, however, we take mass conservation as the only constraint, the problem is greatly simplified. However, this simplification will also cause the model to be unable to simulate the turbulence and surface layer in the flow system. This

question will be addressed in detail in our parameterization of these features in the future research.

There have been many developments of this type of model during the last several decades. Ratto (1996) has provided a recent literature review of mass consistent modeling. In it, he points out that a mass consistent model can provide a performance similar to that of a full dynamical simulation model in some specific applications. Sherman (1978) and Dickerson (1978) have applied mass conservation to an analysis of atmospheric flows over complex terrain. Their model uses a local Cartesian coordinate, and the earth's surface is approximated with a constant step in the vertical direction. The partition of flow into both the vertical and horizontal directions is based on a simple empirical coefficient. Development of other such models by Davis, Bunker, and Mutschlecner (1984) and Ross, Smith, Manins, and Fox (1988) employs a terrain-following sigma z coordinate system. Connell (1988) has done extensive testing on Ross's model using observational data, and her results conclude that the model performed adequately for the flow over a single mountain. The above authors attempted to formulate the flow partition coefficient in terms of the Froude number. Kitada, Igarashi, and Owada (1986) adopted a similar coordinate system in their model and applied it to a land-sea breeze type wind circulation pattern. Moussiopoulos and Flassak (1986) presented a faster numerical algorithm, using a vector computer, to compute the wind field but did not distinguish between the relative adjustment in the horizontal and vertical directions. These models have typically covered 100 x 100 km domains at horizontal resolutions of 2 to 4 kilometers. No approach to date has included the effect of the detailed surface features (morphology), such as buildings and plant canopies, which become important as the resolution is increased. Cionco (1985) has demonstrated, for two dimensional simulations, the effect and impact of surface morphology on the behavior of the near-surface flow as resolution is increased.

The objective in this project is to develop a robust, high-resolution three-dimensional mass consistent diagnostic wind model (3DSTAT) which can be applied in real-time simulations (Mercurio et al., 2001). This model has to be both reasonably accurate in representing the flow physics and computationally efficient. The basic framework of the model is discussed in this document. The planned treatment of the surface roughness layer is described in section 2, the numerical implementation of the model is discussed in section 3, and several idealized tests of the prototype of the model are presented in section 4. The detailed treatment of the surface layer, including the parameterizations of the turbulent surface layer, the flow in plant canopies, the turbulent wakes by the bluff building blocks, and the atmospheric stability effect, will be implemented and described in the future as on-going processes of the model development.

2. Model Description

2.1 Variational Formulation

The model is based on the mass conservation principle, which eliminates the divergence in a flow field. That is, given a limited number of observations or a coarsely modeled wind field over complex terrain, the wind field is physically interpolated in such way that mass conservation is satisfied. Mathematically, the problem is to minimize the functional

$$E(u,v,w,\lambda) = \int_v \left[\beta_1^2 \ (u-u^0)^2 + \beta_1^2 \ (v-v^0)^2 + \beta_2^2 \ (w-w^0)^2 + \lambda\left(\frac{\partial u}{\partial x} + \frac{\partial v}{\partial y} + \frac{\partial w}{\partial z}\right) \right] dxdydz \quad (1)$$

in which x, y are the horizontal coordinates, z the vertical coordinate, u^0, v^0, w^0 the initial observed velocity components, u, v, w the corrected velocity components, λ the Lagrange multiplier, and β_1, β_2 Gauss precision moduli, which are the wind vector partitioning factors in the horizontal and vertical directions, respectively. The Euler-Lagrange equations corresponding to equation (1) are

$$\begin{aligned} u &= u^0 + \frac{1}{2\beta_1^2}\frac{\partial \lambda}{\partial x} \\ v &= v^0 + \frac{1}{2\beta_1^2}\frac{\partial \lambda}{\partial y} \\ w &= w^0 + \frac{1}{2\beta_2^2}\frac{\partial \lambda}{\partial z} \\ \frac{\partial u}{\partial x} + \frac{\partial v}{\partial y} + \frac{\partial w}{\partial z} &= 0 \end{aligned} \quad (2)$$

subject to the boundary conditions

$$\lambda(u-u^0) = 0, \quad \lambda(v-v^0) = 0, \quad \text{and} \quad \lambda(w-w^0) = 0 \quad (3)$$

This corresponds to either setting $\lambda = 0$ ("flow through" free boundaries) or requiring the normal component of the flow at the boundary to remain unchanged after the adjustment.

Equations 2 can be cast into an equation for the Lagrange multiplier, λ, in terms of the initial conditions, by differentiating the equations for u, v, and w, and substituting the results into the continuity equation to give a Poisson equation 4. The β_1 and β_2 values are assumed to be constants throughout the small domain.

$$\frac{\partial^2 \lambda}{\partial x^2} + \frac{\partial^2 \lambda}{\partial y^2} + \left(\frac{\beta_1}{\beta_2}\right)^2 \frac{\partial^2 \lambda}{\partial z^2} = -2\beta_1^2 \left(\frac{\partial u^0}{\partial x} + \frac{\partial v^0}{\partial y} + \frac{\partial w^0}{\partial z}\right) \tag{4}$$

Without altering their physical meaning, let $\alpha = (\beta_1/\beta_2)$ and $\beta_1 = 1$ so that α represents the adjustment of the vertical component relative to the horizontal components (equation 5). Determination of the α value is a complex operation and it is discussed in detail in section 2.4.

$$\frac{\partial^2 \lambda}{\partial x^2} + \frac{\partial^2 \lambda}{\partial y^2} + \alpha^2 \frac{\partial^2 \lambda}{\partial z^2} = -2\left(\frac{\partial u^0}{\partial x} + \frac{\partial v^0}{\partial y} + \frac{\partial w^0}{\partial z}\right) \tag{5}$$

The λ value in equation 5 can be solved numerically by setting the boundary conditions on all facets of the computation domain. The *u, v, w* wind components then can be computed from equation 2 with the λ value solved from equation 5. The iterative convergence will be the high resolution diagnostic solution for *u, v, w* for the given boundary and coarse initial conditions (observations). At the lateral boundaries, λ is set equal to zero to allow "flow through" in the flow adjustment. At the bottom of the domain, "no-flow-through" conditions can be satisfied by having the normal derivative vanish, i.e., $\partial\lambda/\partial z = 0$.

2.2 Vertical Coordinate

In this model, a local Cartesian coordinate (*x,y,z*) has been chosen for the development and testing. The reason is that the objective of the model is to simulate microscale wind flows (10 to 100 m) in complex terrain or around buildings where the computational domain and flow scale are small. In the terrain-following coordinate system, the transformation Jacobian matrix requires the derivative between the coordinate variables to exist in a mathematically continuous (smooth) surface. The discontinuity of sharp corners or vertical walls will cause a singularity in some element of the Jacobian matrix. The sigma z terrain-following coordinate must limit the slope to be less than one vertical grid increment per horizontal increment and cannot represent severe terrain or city buildings. In this prototype of the model, we use a simple Cartesian coordinate. A variable step vertical coordinate following Tripoli, Williamson, and Garvey (2003) will be implemented in the future to better represent the topography. This vertical coordinate system represents a lower boundary by setting the first layer depth to be variable but regularly spaced above. The terrain surface will be described almost exactly as prescribed by the model horizontal resolution, limited by the resolution of the input terrain data. The idea of the variable vertical step grid is illustrated in figure 1. Consider the top of the first building block 1, where the top of the building is a little greater than Z = 2 but less than Z = 2.5. The constant vertical step grid will approximate the building top at Z = 2, but the variable step coordinate will put the building height at a level indicated by placing a variable ΔZ_3 at this first layer.

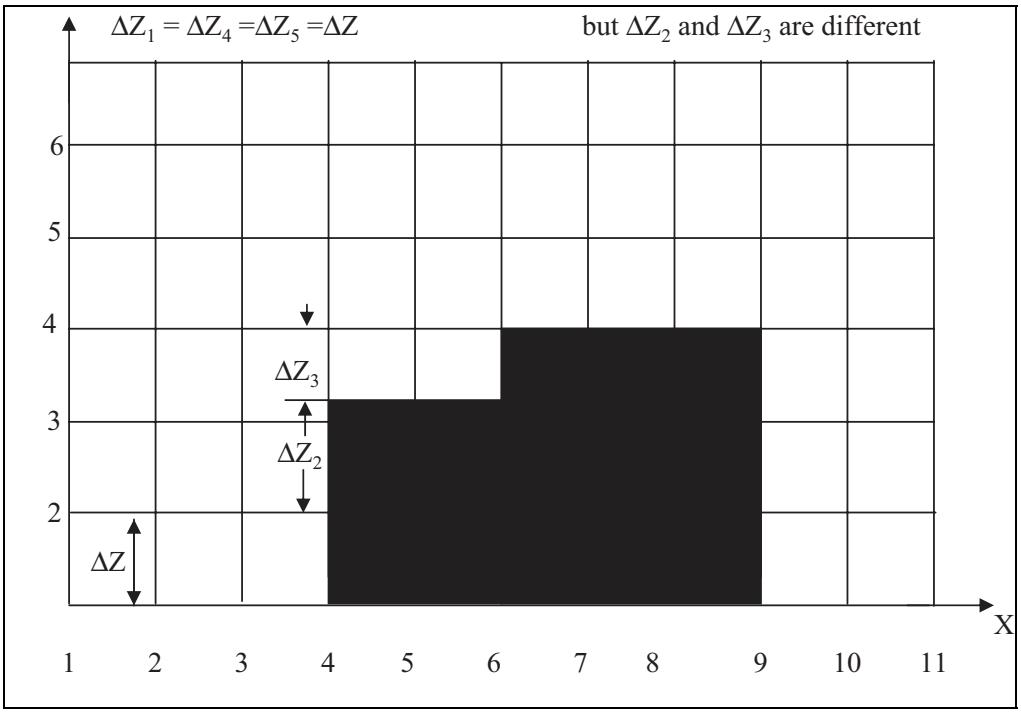

Figure 1. A schematic illustration of variable step vertical coordinate.

2.3 Treatment of the Turbulent Surface Layer

The wind near the earth's surface is highly turbulent and chaotic. Obviously, the mass consistent model will not be able to resolve this flow. The mean surface layer wind characteristics have to be parameterized according to the observational data. For the flow in and just above plant canopies, the vertical wind profile proposed by Cionco (1965; 1985) will be used. The mean wind profile model has been verified through various field experiments (Cionco, 1985; 1999). The simplicity of this relationship allows a straightforward coupling to the 3DSTAT model. The turbulence parameters, such as the momentum and heat fluxes and the standard deviation of wind speed variation, need to be parameterized according to the various field measurements. The flow around and above the building blocks in an urban area also requires special treatment. There are some wind tunnel data (Bossert, Linn, Reisner, Smith, and Winterkamp, 1998; Kastner-Klein, Rotach, Borwn, Fedorovich, and Lawson, 2000; Brown, Lawson, Descroiz, and Lee, 2000) showing the turbulent wakes and boundary separations at the roof top and sidewalls of the buildings. Scarce data are available for actual atmospheric conditions. Planned experiments such as Joint Urban (2003) will supply some data for realistic modeling of the urban wind flow. Since coupling of the turbulent surface layer flow with the upper level flow is a complex topic, a lot of detailed research and study have to be done at this stage. The idea of parameterizing the flow in regions where the model solution is difficult to achieve (or requires very fine resolution) is not novel. This treatment is found in many models, such as boundary layer parameterizations in numerical weather prediction models or logarithmic profile parameterizations in some CFD simulations.

2.4 Partitioning the Flow Using the Richardson Number

The α value in equation 5 defines the flow partitioning between horizontal and vertical motions. The value of α governs the adjustment made in the vertical component relative to the horizontal components. In early mass-consistent models, the value was assumed to be a small constant over the entire domain (Sherman, 1978; Davis et al., 1984) and the value was determined subjectively. Snyder, Thompson, Eskridge, Lawson, Castro, Lee, Hunt, and Ogawa (1985) and Ross, Smith, Manins, and Fox (1988) have related the α value with a hill Froude number to account for the atmospheric stability. Recently, Mercurio, Williamson, Chang, Huynh, Cionco, and Garvey (2001) have proposed relating the flow separation to the bulk Richardson number. This partitioning argument probably makes more sense, considering that the model proposed here is designed to simulate the wind at an even smaller scale than that of the single hill treated by Snyder, Thompson, Eskridge, Lawson, Castro, Lee, Hunt, and Ogawa, (1985) and Ross, Smith, Manins, and Fox (1988). Also, the α value will be larger as the flow scale becomes smaller, since the vertical motion in the microscale flow can become comparable to the horizontal motion. We defer this subject to the next stage of the model development.

3. Numerical Methods

3.1 Finite Difference Discretization

Equation 5 is discretized by a standard 7-point method with second order accuracy in all three spatial directions:

$$\frac{\lambda_{i+1,j,k} - 2\lambda_{i,j,k} + \lambda_{i-1,j,k}}{(\Delta x)^2} + \frac{\lambda_{i,j+1,k} - 2\lambda_{i,j,k} + \lambda_{i,j-1,k}}{(\Delta y)^2} + \alpha^2 \frac{\lambda_{i,j,k+1} - 2\lambda_{i,j,k} + \lambda_{i,j,k-1}}{(\Delta z)^2} = -2f_0 \ , \quad (6)$$

in which f_0 is the divergence of the wind field in the last iteration (or the initial divergence in case of the first iteration), using a central difference in space

$$f_0 = \frac{u^0_{i+1,i,k} - u^0_{i-1,j,k}}{2\Delta x} + \frac{v^0_{i,j+1,k} - v^0_{i,j-1,k}}{2\Delta y} + \frac{w^0_{i,i,k+1} - w^0_{i,j,k-1}}{2\Delta z} \quad (7)$$

The "flow-through" boundary conditions are set by letting $\lambda = 0$, while the "no-flow-through" boundary conditions at the terrain surface and building walls set the normal derivative at the point to zero with a three-point forward (equation 8) and backward difference (equation 9) with second order accuracy.

$$\left(\frac{\partial \lambda}{\partial n}\right)_{m+1} = \frac{3\lambda_{m+1} - 4\lambda_m + \lambda_{m-1}}{2\Delta n} = 0 \quad (8)$$

$$\left(\frac{\partial \lambda}{\partial n}\right)_{m-1} = \frac{-3\lambda_{m-1} + 4\lambda_m - \lambda_{m+1}}{2\Delta n} = 0 \tag{9}$$

Depending on the direction of the normal to the boundary, the appropriate normal direction is denoted by *n*, and the corresponding index is *m*. The adjusted wind field is then computed from the discretized equations of (2) with the α value:

$$u_{i,j,k} = \frac{1}{4}(u^0_{i+1,j,k} + 2u^0_{i,j,k} + u^0_{i-1,j,k}) + \frac{1}{4\Delta x}(\lambda_{i+1,j,k} - \lambda_{i-1,j,k})$$

$$v_{i,j,k} = \frac{1}{4}(v^0_{i,j+1,k} + 2v^0_{i,j,k} + v^0_{i,j-1,k}) + \frac{1}{4\Delta y}(\lambda_{i,j+1,k} - \lambda_{i,j-1,k}) \tag{10}$$

$$w_{i,j,k} = \frac{1}{4}(w^0_{i,j,k+1} + 2w^0_{i,j,k} + w^0_{i,j,k-1}) + \frac{1}{4\alpha^2\Delta z}(\lambda_{i,j,k+1} - \lambda_{i,j,k-1})$$

The convergence to the final values of *u, v, w* is achieved by the iteration of equations 6 to 10 with a prescribed error tolerance. The largest computational load (99%) arises in solving the three-dimensional Poisson equation to determine the λ values. The multigrid method described in the next sub-section is employed to accelerate the computation of the Poisson equation.

3.2 Multigrid Method

The discretization of the Poisson equation in a Cartesian grid leads to a system of linear difference equations. This equation set is non-symmetric, diagonally dominant, and locally dependent on the terrain. Since the equation set is a very large system (e.g., 129^3 x 129^3 matrix for a 129 x 129 x 129 grid), an iterative method must be applied to solve the equation set. The over-relaxation iteration method was initially applied for this purpose. However, the over-relaxation method is quite slow to converge. Multigrid algorithms are effective and fast in the solution of elliptic equations, and they have recently found many other applications. In many cases, the multigrid method is considered as the optimal method to solve the elliptical differential equation.

In the tutorial by Briggs, Henson, and McCormick (2000), the multigrid method was introduced as a means to accelerate the convergence of the relaxation procedure. Many relaxation schemes have a smoothing property, so that the high frequency oscillatory modes of the error are eliminated effectively, but lower frequency smooth modes are dampened only slowly. The smoothness of the error is relative to the computational grid size, and a smooth mode in a fine grid appears to be high frequency to a coarse grid. The multigrid method takes advantage of this property to accelerate the convergence by dealing with the low frequency error in coarser grids. The multigrid method uses coarser grids recursively to relax the smooth mode error and interpolate back to the finer grid. Coarse grids are also used to compute an improved initial guess for the fine grid relaxation. The full multigrid method (FMG) applied in this numerical model can be described as follows:

In order to describe the FMG algorithm clearly, a two-grid correction scheme is described, first as one-dimensional. The three-dimensional multigrid method is then a simple extension of the one dimensional problem. The FMG V-cycle scheme is used here to solve the finite difference equation $L\lambda = f$ at grid size $h = \Delta x$, where L is a one-dimension Poisson operator (second derivative). An appropriate two-grid correction scheme is

1. Relax γ_1 times on $L^h \lambda^h = f^h$ on fine grid ($\Delta x = h$) with a given initial guess μ^h.
2. Compute the fine grid residual $r^h = f^h - L^h \mu^h$ and average it to the coarse grid.
3. Solve the residual equation $L^{2h} e^{2h} = r^{2h}$ for e^{2h} on coarse grid ($\Delta x = 2h$).
4. Interpolate the coarse grid error to the fine grid and then correct the fine grid approximation. $\mu^h \leftarrow \mu^h + e^h$.
5. Relax γ_2 times on $L^h \lambda^h = f^h$ on the fine grid with initial guess μ^h

With the two-grid method in mind, it is a short step to the multigrid method. Instead of solving the coarse grid residual equation exactly, we can get an approximate solution of it by introducing an even coarser grid and using the two-grid method. This idea can be applied recursively down to some coarsest grid, where the solution of the error can be found easily by direct matrix inversion or iteration. The iteration of a multigrid method from finest grid to coarsest grid and back to finest grid again is called a cycle. If the two-grid iteration at each intermediate grid is executed once only, it is called a V cycle.

The FMG V-cycle is a further extension of the V cycle described before. Instead of starting with an arbitrary approximation on the finest grid, which is usually a poor guess, we start to solve the liner system at the coarsest grid and use that solution to provide a better guess for the initial field on the next finer grid. This operation is conducted to the finest grid for a good starting guess of the solution at each grid level. This nested iteration to find the initial guess can greatly increase the efficiency of the multigrid method.

The interpolation method applied in the three-dimensional FMG method is a simple trilinear interpolation. The corresponding averaging method is a fully weighted average. With three-dimensional stencil notation, the trilinear interpolation (operator P) from coarse grid to fine grid can be described in the following equations (Wesseling, 1992):

$$
\begin{aligned}
(P\lambda)_{2i} &= \lambda_i \\
(P\lambda)_{2i+e1} &= \frac{1}{2}(\lambda_i + \lambda_{i+e1}) \\
(P\lambda)_{2i+e1+e2} &= \frac{1}{4}(\lambda_i + \lambda_{i+e1} + \lambda_{i+e2} + \lambda_{i+e1+e2})
\end{aligned}
\tag{11}
$$

$$(P\lambda)_{2i+e1+e2+e3} = \frac{1}{8}(\lambda_i + \sum_{j=1}^{3} \lambda_{i+e_j} + \lambda_{i+e1+e2} + \lambda_{i+e2+e3} + \lambda_{i+e3+e1} + \lambda_{i+e1+e2+e3})$$

in which $e1$, $e2$, and $e3$ are the unit directional vectors, defined as

$$e1 = (1,0,0), \quad e2 = (0,1,0), \quad e3 = (0,0,1) \tag{12}$$

The restriction or averaging operator (R) is an adjoint of the operator P, which is a fully weighted average in the neighboring points. The weighting factors for the 27 points in the three-dimensional stencil are expressed as three slices of matrix:

$$R^{(-1)} = R^{(1)} = \frac{1}{8}\begin{pmatrix} 2 & 4 & 2 \\ 4 & 8 & 4 \\ 2 & 4 & 2 \end{pmatrix} \quad \text{and} \quad R^{(0)} = \frac{1}{8}\begin{pmatrix} 1 & 2 & 1 \\ 2 & 4 & 2 \\ 1 & 2 & 1 \end{pmatrix} \tag{13}$$

in which $R^{(0)}$ is the center slice that passes through the center point, and $R^{(1)}$ and $R^{(-1)}$ are the first and third slices.

The trilinear interpolation and the fully weighted average preserve symmetry but are more expensive compared to other operators such as simple interpolation and simple injecting. A detailed description of the interpolation and averaging operators is presented in Wesseling (1992).

The relaxation method to solve the linear system equation is the red-black Gauss-Seidel method. The Gauss-Seidel scheme is

$$\lambda_i = -\frac{1}{L_{ii}}(\sum_{\substack{j=1 \\ j \neq i}}^{n} L_{ij}\lambda_j - f_i) \qquad i = 1,...,N \tag{14}$$

in which the N is the number of grid points in a specific grid. The grid points are ordered in a checker board fashion in the alternating red and black order, and the revising of the red point only uses values at the black point, and vice versa. The red and black points are completely decoupled and the revising of both groups may be done in parallel. This property is certainly beneficial on parallel computers (Press, Flannery, Teukolsky, and Vetterling, 1992). The convergence theory for the multigrid method is beyond the scope of this report, and the reader is referred to Wesseling (1992) and Briggs, Henson, and McCormick (2000).

The interpolation, averaging, and relaxation operator use exactly the same subprogram at every grid level. The numerical routines are implemented via a standard FORTRAN (Formula Translator) 90 code structure. The dynamical memory allocation and the recursive subroutine are used to improve the efficiency of the numerical code.

4. Initial Test Results of the Model

4.1 Test With the Potential Flow Solutions

The model formulation and coding require very rigorous testing to detect potential coding errors. A logical first test is to compare with analytical solutions if available. The model formulation of the minimization of the functions resulted in a Poisson equation 5 with respect to the Lagrange multiplier λ. By letting α = 1 (the wind is adjusted equally in the vertical and horizontal directions), equation 5 can rewritten in vector form:

$$\nabla^2 \lambda = -2\nabla \bullet \vec{V}_0 \tag{15}$$

The λ represents a velocity potential for non-viscous, irrotational flow if the initial wind divergence $\nabla \bullet \vec{V}_0 = 0$. This condition is satisfied for the uniform background wind. Thus, a mass consistent numerical model simulation of an initially uniform wind flow over a terrain is equivalent to the potential flow solution. The potential flow can be expressed in a more general sense (Ross, Smith, Manins, and Fox, 1988): If the initial wind $\vec{V}_0 = (u_0, v_0, w_0)$ can be separated as

$$u_0 = u_0(x), \quad v_0 = v_0(y) \quad \text{and} \quad w_0 = w_0(z) \tag{16}$$

then the final wind satisfies a velocity potential Φ

$$u = \frac{\partial \Phi}{\partial x}, \qquad v = \frac{\partial \Phi}{\partial y}, \qquad w = \frac{\partial \Phi}{\partial z} \tag{17}$$

in which

$$\Phi = \int u_0 dx + \int v_0 dy + \int w_0 dz + \frac{\lambda}{2} \ . \tag{18}$$

We then have an equation that is identical with (15)

$$\nabla^2 \Phi = \nabla \bullet \vec{V}_0 + \frac{1}{2}\nabla^2 \lambda = 0 \tag{19}$$

There are some analytical solutions for the potential flow around simple two-dimensional or three-dimensional geometrical objects such as a cylinder, sphere, or ellipse (Milne-Thompson, 1960). However, for complex geometrical obstacles, analytical solutions are not possible and numerical simulation is the preferred method. Nevertheless, the simple geometry analytical solutions are useful for the testing of the numerical model. The following are some model tests compared to some simple potential flow analytical solutions. The potential flow theory is a good approximation for the flow over an obstacle in the neutral condition and when the Froude

number (*Fr)* is much greater than 1, except in the region of turbulent wake in the lee side of the flow. The Froude number is defined as

$$F_r = \frac{V_\infty}{Nh} \tag{20}$$

in which V_∞ is the uniform wind speed approaching the hill, *h* is the height of the hill, and $N = \sqrt{-\frac{g}{\rho}\frac{d\rho}{dz}}$, the Brunt-Väisälä frequency. The condition of $F_r >> 1$ can be found in the condition when (1) there is a homogenous and well-mixed condition ($N \to 0$) in which the Reynolds number is usually large (Baines, 1995), or (2) a small hill height (h), given the flow is stratified. The parameterization of the lee side turbulence will be studied in detail in the next stage of the research. The potential flow theory is to be compared here only for the purpose of checking the computational methods and the flow upstream and above the turbulence wake.

a. Potential Flow Over a Hemisphere

A simple hemisphere with a radius of 2.5 km is used for this case. The potential flow analytical solution for this case is an axis symmetric flow in a polar coordinate (*r,θ*) (Milne-Thompson, 1960):

$$\begin{aligned} V_r &= V_\infty \cos\theta\left(1 - \frac{r^3}{a^3}\right) \\ V_\theta &= -V_\infty \sin\theta\left(1 + \frac{r^3}{2a^3}\right) \end{aligned} \tag{21}$$

in which V_r and V_θ are the wind velocity components normal and tangential to the hemisphere surface, respectively, θ is the elevation angle of the line normal to the point, V_∞ is the uniform prescribed wind speed, *a* is the distance from the hemisphere center, and *r* is the radius of the hemisphere. The potential solution is simulated with the 3DSTAT model on a 10-km x 10-km x 10-km domain. The grid number is 129 x 129 x 129 and dx = dy = dz = 77.5m. The radius of the hemisphere is 2.5 km and the uniform wind speed is 10 m/s. The comparison of the analytical solution and the numerical solution is plotted in figure 2. The left panel is the analytical solution and the right panel is the 3DSTAT simulation. In both solutions, the top panel displays the horizontal cross section at z = 1.55 km and the bottom panels shows the vertical cross section at y = 5 km. Overall, the numerical simulation captured the potential flow solution and showed the wind turning, climbing, accelerating on the mountain top, and approaching zero at the stagnation point.

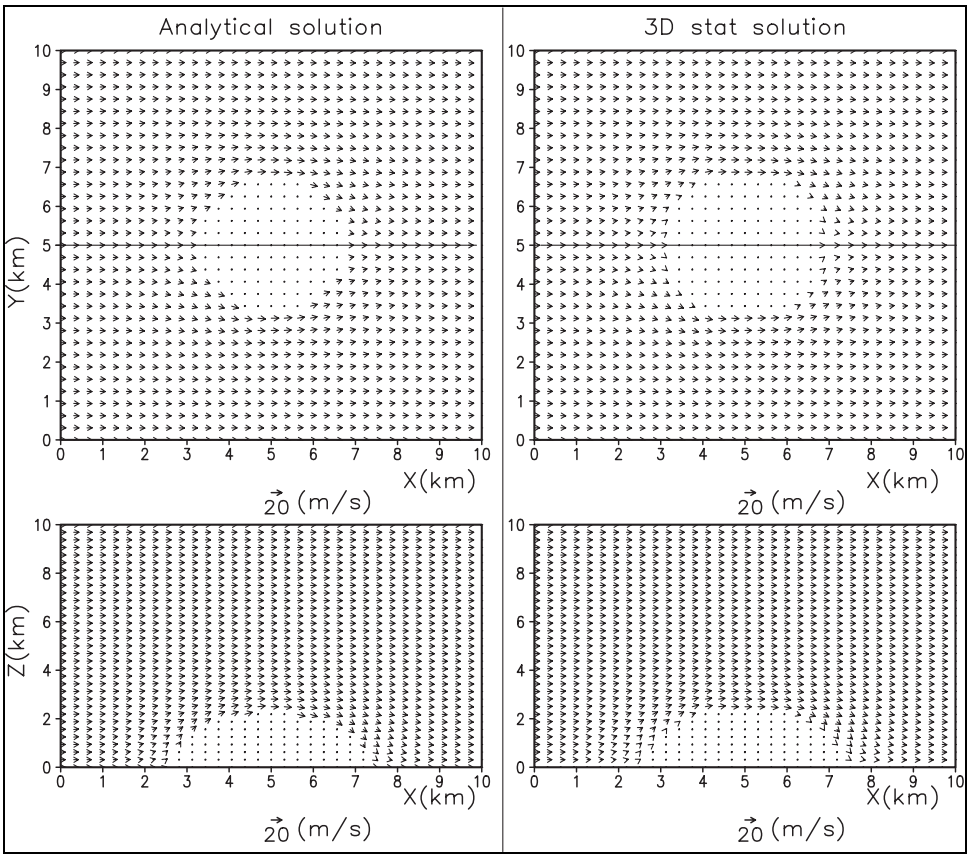

Figure 2. Comparison of the potential flow analytical solution (left panel figures) with the numerical model solution (right panel figures). (The top panels are the horizontal cross sections at z = 1.55 km. The bottom panels are the vertical cross sections at y = 5 km.)

b. Potential Flow Over Two-Dimensional Ridges

There are potential flow solutions for many two-dimensional geometries. Two have been chosen for the purpose of testing the model. The flow over the half cylinder and the flow over a two-dimensional "Witch-of-Agnesi" (representing long ridges in the y direction), are presented here. An important feature for stratified flow over those types of ridges (Queney, 1948; Long, 1953) and over a three-dimensional Witch-of-Agnesi (Smith, 1989) is that solutions based on linear perturbation theory show gravity waves generating along the lee side of the ridges for large Froude numbers. The diagnostic model presented here will not show this type of waves because it does not address momentum conservation. However, for a small obstacle or for the well-mixed atmospheric condition, the potential flow is a valid approximation except in the a flow separation region such as lee wake. Figure 3 compares the potential flow analytical solutions (Milne-Thompson, 1960; Queney, 1948) and the 3DSTAT simulation. The top panel is for the flow over a half cylinder and the bottom panel for the flow over the two-dimensional Witch-of-Agnesi ridge. The streamlines in both simulations match the analytical solution reasonably well. However, the model simulations have some differences near the surface of these ridges.

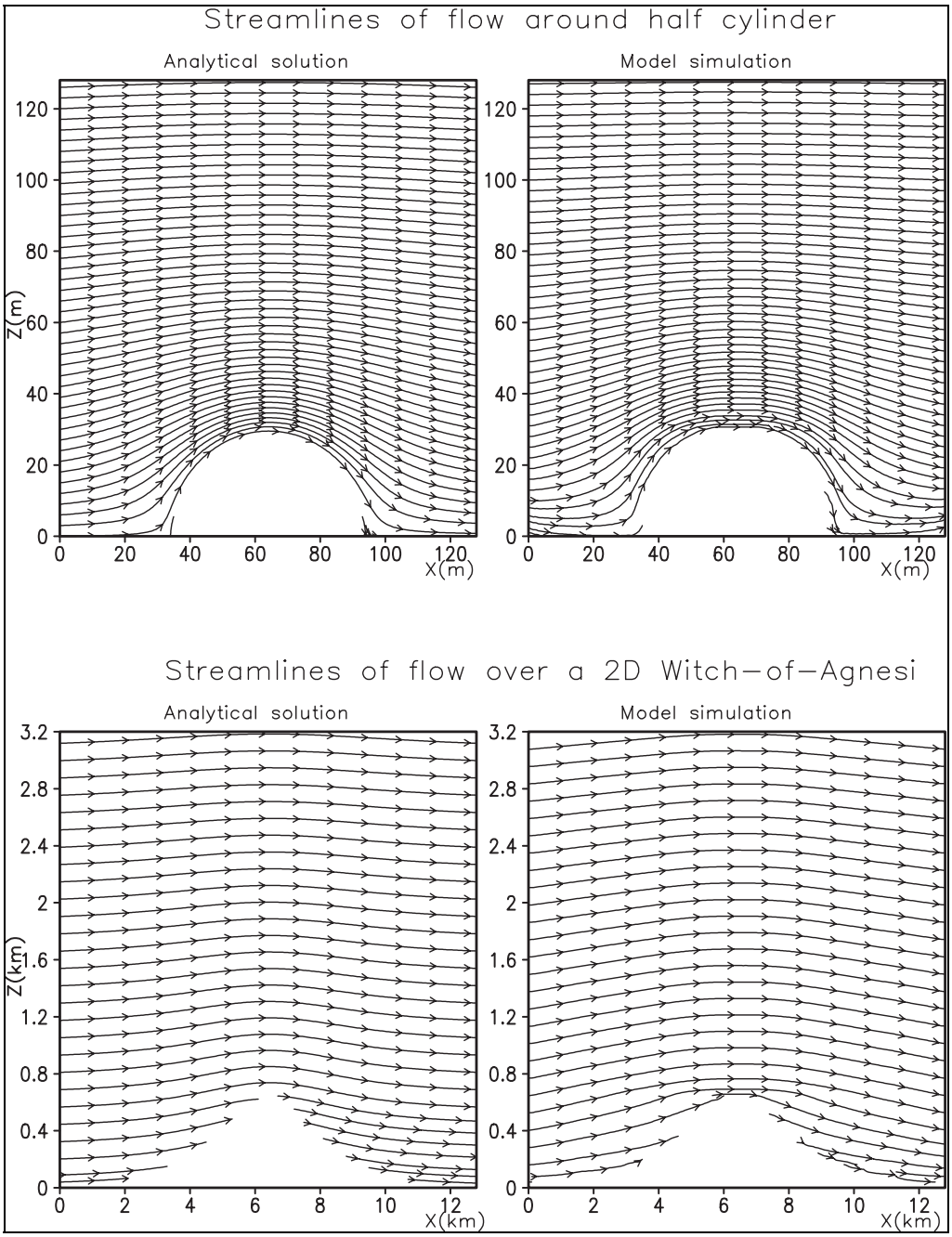

Figure 3. Streamlines of flow around infinite long half cylinder ridge (top panel); streamlines of flow over a 2-D Witch-of-Agnesi ridge (bottom panel).

4.2 Flow Around and Over Building Blocks

Wind flow around building blocks or building canyons is a very complex problem. There have been a number of wind tunnel studies and reviews of wind flow around simple obstacles (Hunt, Abell, Peterka, and Woo, 1978) or groups of building blocks (Bossert, Linn, Reisner, Smith, and Winterkamp 1998; Kastner-Klein, Rotach, Brown, Fedorovich, and Lawson 2000; Brown, Lawson, Descroiz, and Lee, 2000). For an isolated cubical obstacle, Hunt, Abell, Peterka, and

Woo, (1978) showed that several areas in the immediate vicinity of the obstacle have re-circulations and higher turbulent intensities because of the steep sides and sharp corners (figure 4). On the central plane of symmetry of fluid flow past a cuboid there are the upstream re-circulation region, the roof-separated flow region, and the main wake with reversed flow on the lee side. At the side walls, there are also flow separations. Brown, Lawson, Descroiz, and Lee (2000) showed that when a wind flowed perpendicularly over a seven-building array, the flow separated at the top of the first building but not over the remaining downstream buildings. The flow at the surface was nearly identical in all street canyons, where there was a re-circulation region with a strong reversed flow at 0.6 building height.

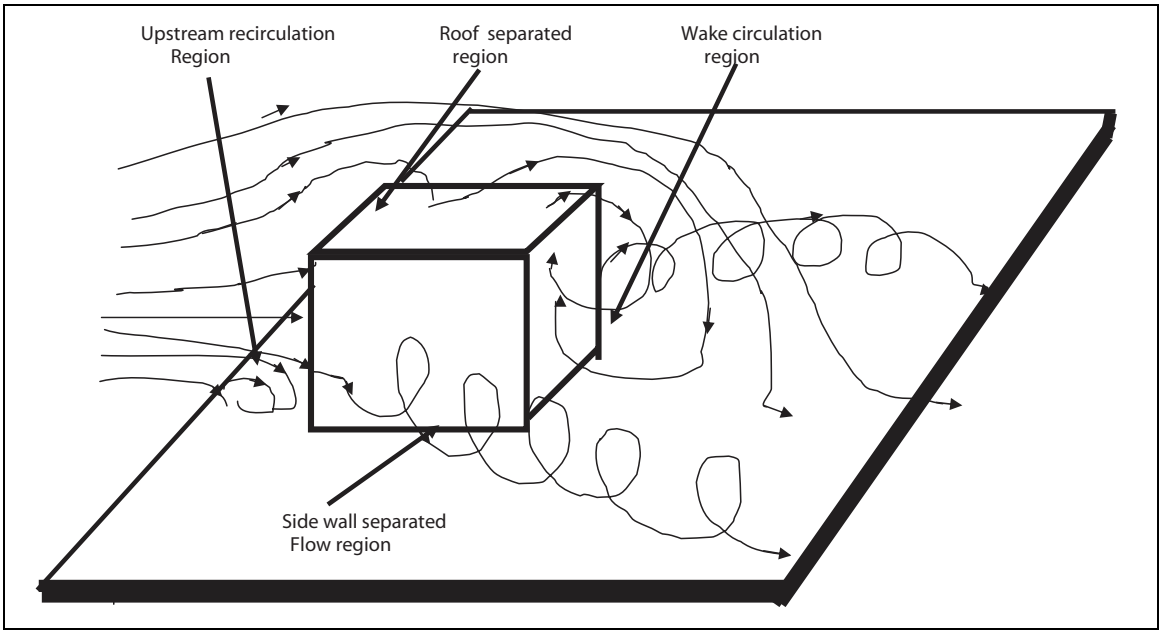

Figure 4. A schematic graph shows the mean flow pattern over and around a wall-mounted box.

Figure 5 shows the 3DSTAT simulation (top panel) of the flow over three building blocks compared with the wind tunnel results. Obviously, we do not expect the 3DSTAT model to simulate the canyon vortex and the boundary layer separation at the top of the first building because the model does not contain the momentum conservation. The flow outside these regions, which can be approximated by the potential flow theory (Baines, 1995), is similar to the wind tunnel results. The wake area and the flow separation area have to be parameterized in further model development. Figure 6 shows another 3DSTAT solution for the wind flow around and above a group of five buildings. The first two buildings on the left (see the top panel) are 13 meters high, while the others are 8 meters high. The streamlines show that the 3DSTAT simulation captured the expected flow around the buildings (top panel) and the building blocking effects. The bottom panel shows the flow over the vertical cross section at y = 30m. The wind at the top building also shows acceleration. However, the wakes at the lee side of the buildings are not simulated because momentum conservation is not imposed.

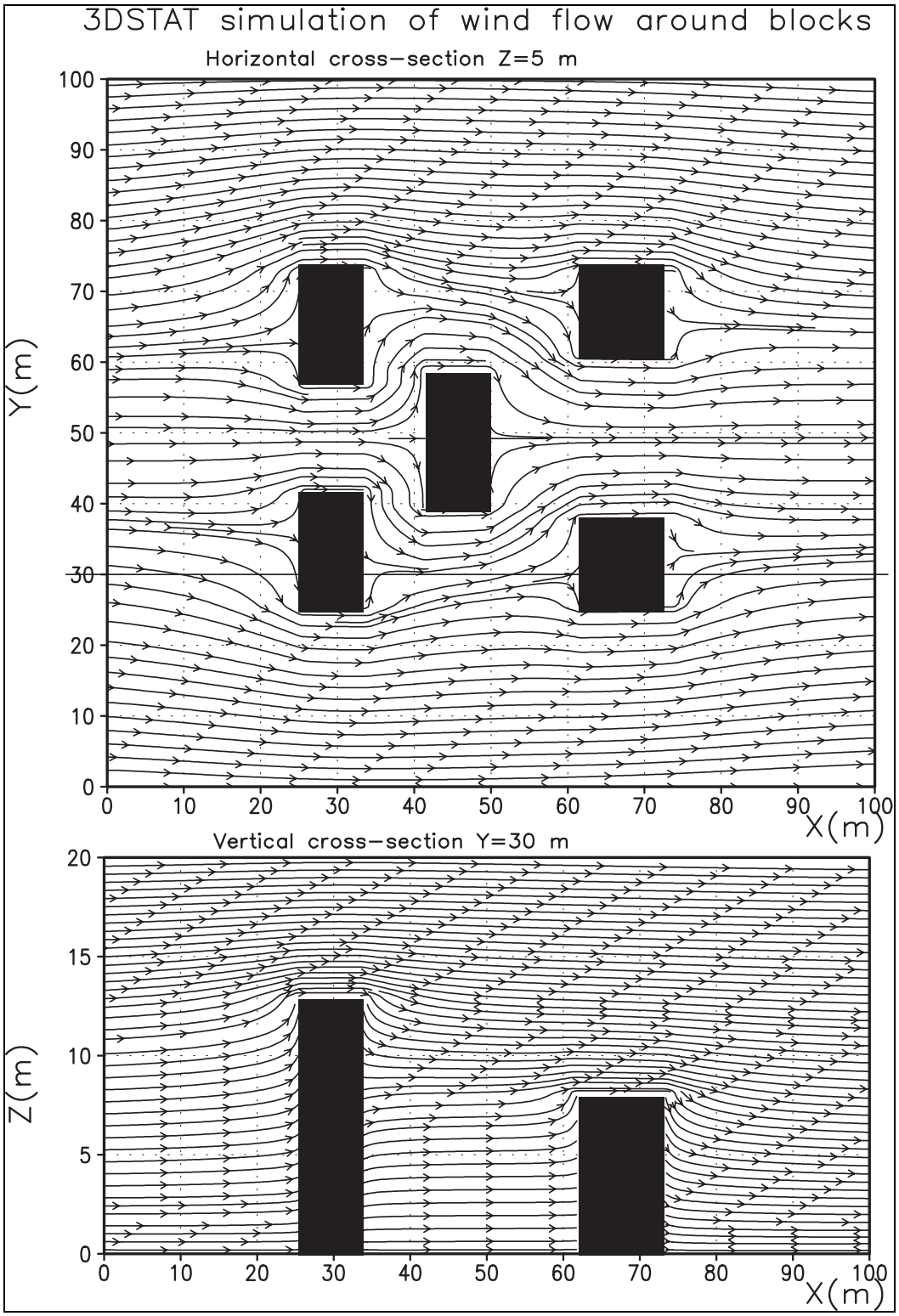

Figure 5. 3DSTAT simulation of wind flow around and over 3-D building blocks. (The top panel is a horizontal cross section at z = 5m, and the bottom panel is a vertical cross section at y = 30m.)

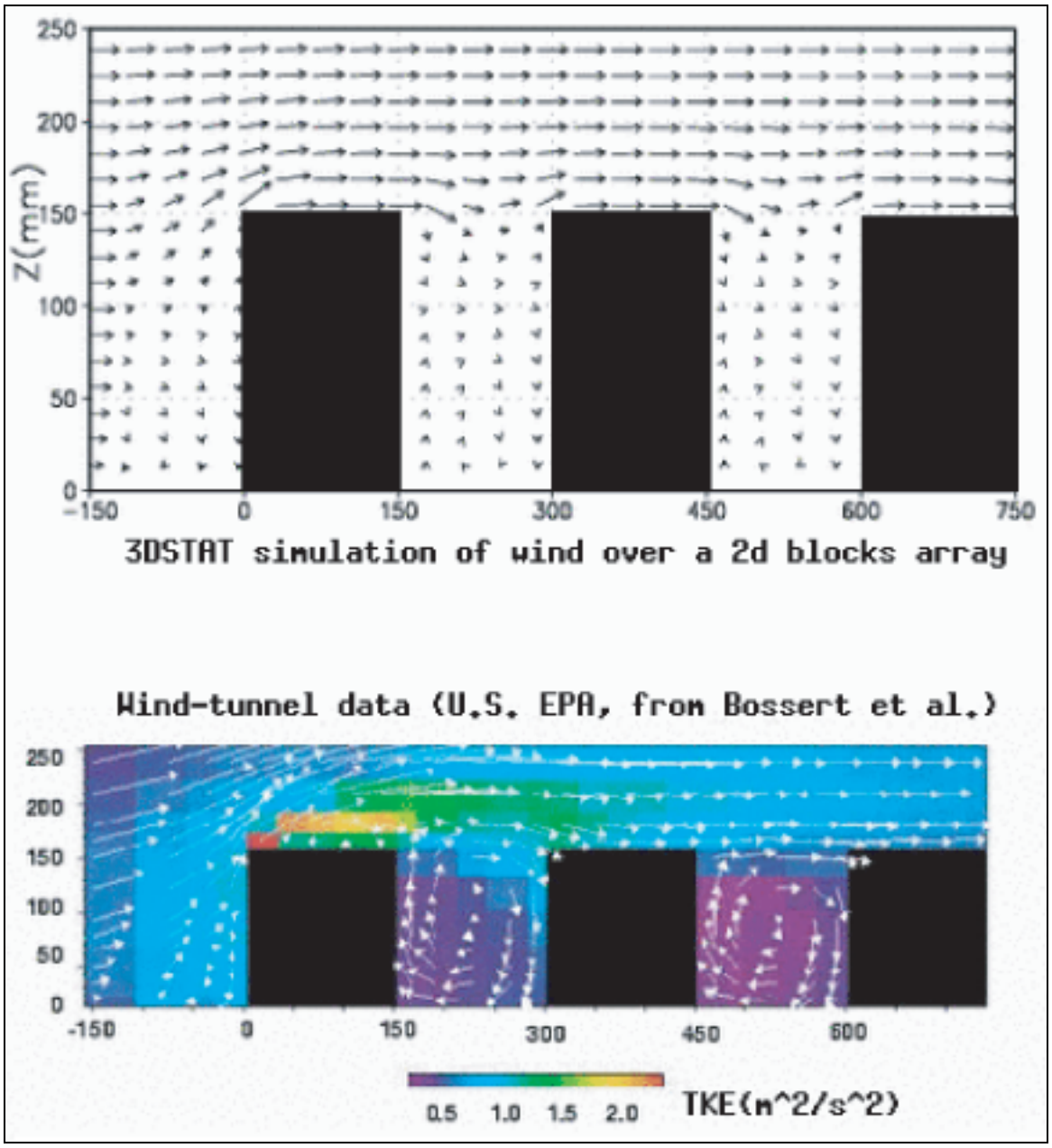

Figure 6. Flow over a 3-D block array. (3DSTAT simulation (top panel) and the wind tunnel data (bottom panel, U.S. EPA)).

4.3 Computational Efficiency of the Model

The multigrid method applied in the computation very much improves the computational efficiency. Before implementation of the multigrid method, we developed a test version of the model use a simple red-black (RB) Gauss-Seidel over-relaxation method to solve the Poisson equation. Table 1 lists the control processing unit (CPU) times required for the test cases with both versions of the model. The testing was done on a two-processor 2-GHz Pentium 4 Linux Dell computer. Basically, this version of the model takes about 20 to 30 times more CPU time to

run, compared with the latest model version implemented with the multigrid model (depending on the complexity of the underlying terrain). Another advantage of the multigrid method is that the computation time is not proportionally increased as the terrain surface becomes more complex. Indeed, test case 2 over case 4 only showed about a 1.5-minute CPU time increase in the multigrid version model, while it had a 2-hour increase of CPU time with the simple RB Gauss-Seidel over-relaxation. We have tested this code for scalability for multiprocessor computers using a simple OpenMP compiling option. The results showed that the code scales fairly well up to four processors with about a 1.8 time acceleration. Indeed, the RB Gauss-Seidel relaxation has very good properties when the red and black points are decoupled so that parallel processing can be easily applied.

Table 1. Comparison of CPU time (minutes) with different numerical methods.

Test Cases	Topographies	Simple RB Gauss-Seidel method	Multigrid method
1	Hemisphere (3D)	124	6
2	Half-cylinder (2D)	119	6.4
3	Witch-of-Agnesi (2D)	120	7.1
4	Building array (2D)	218	7.5
5	Five buildings (3D)	207	7.8

5. Summary and Conclusions

This document describes a prototype high resolution, three-dimensional, computationally efficient, diagnostic model for flow over complex terrain with a mass-consistent approach. The differences between the current model and similar approaches are in the vertical coordinate, the lower boundary conditions, and the choice of numerical method. This model will use a step vertical coordinate which is better suited for very steep topography and will include the effects of not only topography but also small surface features such as trees and buildings on the overall flow. The numerical implementation takes advantage of a multigrid method which greatly improves the computation speed. The framework of the model and associated implementations have been described here, several preliminary test cases for the model have been demonstrated, and deficiencies of the model have been addressed. The proposed parameterization of the turbulent surface layer and the flow partition will be performed in our future research with field observation data.

References

Baines, P. G. *Topographic effects in stratified flows*; Cambridge Univ. Press. 1995.

Briggs, W. L.; Henson, V. E.; McCormick, S. F. *A multigrid tutorial*; SIAM publishing. 2000.

Bossert, J. E.; Linn, R. R.; Reisner, J. M.; Smith, S.; Winterkamp, J. *Advances in Microscale atmospheric modeling*. Earth and Environmental Sciences Progress Report 1998-2000, Los Alamos National Laboratory, 1998.

Brown, M. J.; Lawson, R. E.; Descroix, D. S.; Lee, R. L. Mean flow and turbulence measurements around a 2-D array of buildings in wind tunnel. *11th conf. On Appl. of Air Poll. Meteorol.*, Long Beach, CA. January 2000; Amer. Meteorol. Soc. Boston.

Cionco, R. M. A mathematical model for air flow in the vegetative canopy. *J. Appl. Meteorl*. **1965**, *4*, 517.

Cionco, R. M. *Modeling windfields and surface layer wind profiles over complex terrain and within vegetative canopies*; The Forest-Atmosphere Interaction, B. A. Hutchison and B. B. Hicks(eds); Reidel Publishing Company, 1985; p 501-520.

Cionco, R. M.; aufm Kampe, W.; Biltoft, C.; Byers, J. H.; Collins, C. G.; Higgs, T. J.; Hin, A.R.T.; Johansson, P.-E.; Jones, C. D.; Jørgensen, H. E.; Kimber, J. F.; Mikkelsen, T.; Nyrén, K.; Ride, D. J.; Robson, R.; Santabarbara, J. M.; Streicher, J.; Thykier-Nielsen, S.; van Raden, H.; Weber, H. An overview of MADONA: A multinational field study of high resolution meteorology and diffusion over complex terrain. *Bull. Amer. Meteorl. Soc*. **1999**, *80*, pp 5-19.

Connell, B. H. 1988: Evaluation of a 3-D diagnostic wind model: NUATMOS. M.S. Thesis, Colorado State Univ., 135 pp.

Davis, C. G.; Bunker, S. S.; Mutschlecner, J. P. Atmospheric transport models for complex terrain. *J. Climate Appl. Meteorol*. **1984**, *23*, pp 235-238.

Dickerson, M. H. MASCON-A mass consistent atmospheric flux model for regions with complex terrain. *J. Appl. Meteorol*. **1978**, *17*, pp 241-253.

Hunt, J.C.R.; Abell, C. J.; Peterka, J. A.; Woo, H. Kinematical studies of the flows around free or surface-mounted obstacles: applying topology to flow visulization. *J. Fluid Mech*. **1978**, *86*, pp 179-200.

Kastner-Klein, P.; Rotach, M. W.; Brown, M. J.; Fedorovich, E.; Lawson, R. E. 2000: Spatial variability of mean flow and turbulence fields in street canyons. *11th conf. On Appl. of Air Poll. Meteorol*., Long Beach, CA. Jan. 2000. Amer. Meteorol. Soc. Boston.

Kitada, T.; Igarashi, K.; Owada, M. Numerical analysis of air pollution in a combined field of land/sea breeze and mountain/valley wind. *J. Climate Appl. Meteorol*. **1986**, *25*, pp 767-784.

Long, R. R. Some aspects of stratified fluids, I. A theoretical investigation, *Tellus* **1953**, *5*, pp 42-58.

Mercurio, J. J.; Williamson, C. C.; Chang, S.; Huynh, G.; Cionco, R. M.; Garvey, D. M. 2001: 3DSTAT- A High resolution 3-D Diagnostic Meteorological model. Battlespace Atmospheric and Cloud Impacts on Military Operations Conference, 10-12 July, Ft. Collins, Co.

Milne-Thompson, L. M. 1960: Theoretical Hydrodynamics, fourth ed., Macmillan Publ. Co.

Moussiopoulos, N.; Flassak, Th. Two vectorized algorithms for the effective calculation of mass-consistent flow fields. *J. Climate Appl. Meteorol*. **1986**, *25*, pp 847-857.

Press, W. H.; Flannery, B. P.; Teukolsky, S. A.; Vetterling, W. T. 1996: Numerical recipes in FORTRAN 90: The art of PARALLEL scientific computing. Cambridge Univ. Press, New York.

Queney, P. The problem of airflow over mountains: A summary of theoretical studies. *Bull. Amer. Meteorpl. Soc*. **1948**, *29*, pp 16-26.

Ratto, C. F. 1996: An overview of mass-consistant models. In "Modeling of Atmosphere Flow Fields", Eds D. P. Lalas and C. F. Ratto., World Scientific Publications. pp 379-400.

Ross, D. G.; Smith, I. N.; Manins, P. C.; Fox, D. G. Diagnostic wind field modeling for complex terrain: Model development and testing. *J. Appl. Meteorol*. **1988**, *27*, 785-796.

Sasaki, Y. An objective analysis based on the variational method. *J. Meteorl. Soc. Japan* **1958**, *36*, pp 77-78.

Sasaki, Y. Some basic formalisms in numerical variational analysis. *Mon. Wea. Rev*. **1970**, *98*, pp 875-883.

Sherman, C. A. A mass-consistent model for wind field over complex terrain. *J. Appl. Meteorol*. **1978**, *17*, pp 312-319.

Smith, R. B. Hydrostatic airflow over mountains. *Advances in Geophysics* **1989**, *31*, pp 1-41.

Snyder, W. H.; Thompson, R. S.; Eskridge, R. E.; Lawson, R. E.; Castro, I. P.; Lee, J. T.; Hunt, J.C.R.; Ogawa, Y. The structure of strongly stratified flow over hills: The dividing-streamline concept. *J. Fluid Mech*. **1985**, *152*, pp 249-288.

Tripoli, G. J.; Williamson C. C.; Garvey, D. A scalable nonhydrostatic model featuring variable step topography. Army Science Conference, Orlando, Florida. 2003.

Wesseling, P. *An introduction to multigrid methods*, John Wiley & Sons. New York,1992.

Intentionally Left Blank.

Distribution

DARPA
ATTN S Welby
3701 N Fairfax Dr
Arlington VA 22203-1714

Ofc of the Secy of Defns
ATTN ODDRE (R&AT)
The Pentagon
Washington DC 20301-3080

US Army TRADOC
Battle Lab Integration & Techl Dirctrt
ATTN ATCD-B
10 Whistler Lane
FT Monroe VA 23651-5850

Dir for MANPRINT
Ofc of the Deputy Chief of Staff for Prsnnl
ATTN J Hiller
The Pentagon Rm 2C733
Washington DC 20301-0300

US Military Acdmy
Mathematical Sci Ctr of Excellence
ATTN LTC T Rugenstein
Thayer Hall Rm 226C
West Point NY 10996-1786

SMC/CZA
2435 Vela Way Ste 1613
El Segundo CA 90245-5500

TECOM
ATTN AMSTE-CL
Aberdeen Proving Ground MD 21005-5057

US Army ARDEC
ATTN AMSTA-AR-TD
Bldg 1
Picatinny Arsenal NJ 07806-5000

US Army Avn & Mis Cmnd
ATTN AMSMI-RD W C McCorkle
Redstone Arsenal AL 35898-5240

US Army Info Sys Engrg Cmnd
ATTN AMSEL-IE-TD F Jenia
FT Huachuca AZ 85613-5300

US Army Natick RDEC
Acting Techl Dir
ATTN SBCN-T P Brandler
Kansas Street Bldg 78
Natick MA 01760-5002

US Army Simulation Train & Instrmntn Cmnd
ATTN AMSTI-CG M Macedonia
ATTN J Stahl
12350 Research Parkway
Orlando FL 32826-3726

US Army Tank-Automtv Cmnd RDEC
ATTN AMSTA-TR J Chapin
Warren MI 48397-5000

Hicks & Assoc Inc
ATTN G Singley III
1710 Goodrich Dr Ste 1300
McLean VA 22102

Director
US Army Rsrch Lab
ATTN AMSRL-RO-D JCI Chang
ATTN AMSRL-RO-EN W D Bach
PO Box 12211
Research Triangle Park NC 27709

US Army Rsrch Lab
ATTN AMSRL-D D R Smith
ATTN AMSRL-D J M Miller
ATTN AMSRL-CI-EA D Garvey
ATTN AMSRL-CI-EB C Williamson
ATTN AMSRL-CI-EB S Chang
ATTN AMSRL-CI-EB Y Wang
ATTN AMSRL-CI-EE J Mercurio
ATTN AMSRL-CI-IS-R Mail & Records Mgmt
ATTN AMSRL-CI-IS-T Techl Pub (2 copies)
ATTN AMSRL-CI-OK-TL Techl Lib (2 copies)
Adelphi MD 20783-1197

Intentionally Left Blank.